Supplementary Information

Rapid Emission–Economy Decoupling alongside the Urbanization of Chinese Counties

Hao Kong[†], Jintai Lin[*,†,‡], Sijie Wang[†], Ruijing Ni[§], Yuhang Zhang[†], Mengying Wang[†], Chenghao Xu[†]

[†]Laboratory for Climate and Ocean-Atmosphere Studies, Department of Atmospheric and Oceanic Sciences, School of Physics, Peking University, Beijing, 100871, China

[‡]Institute of Carbon Neutrality, Peking University, Beijing, 100871, China

[§]Sichuan Academy of Environmental Policy and Planning, Sichuan, 610093, China

The Supplementary Information includes 19 pages, 15 figures and 3 tables.

Figures

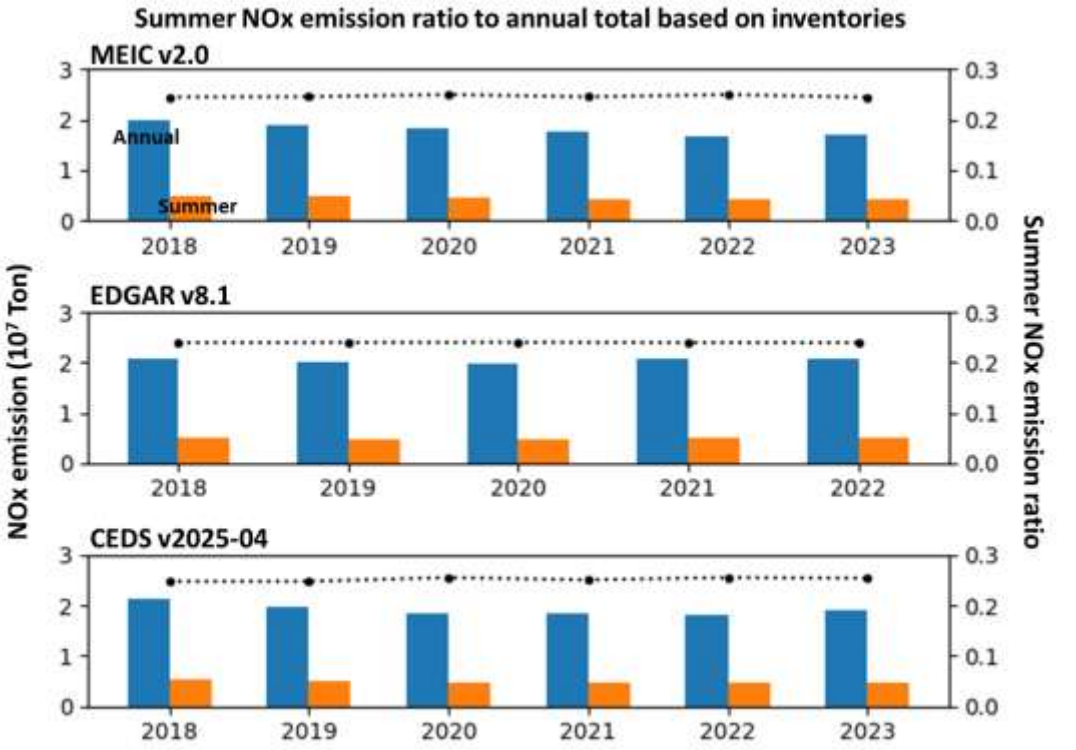


Figure S1. Summer NO_X emission ratios in each year based on inventories. Summer refers to June, July, and August. The inventories include MEIC v2.0 (last access: March 23, 2026), EDGAR v8.1 (last access: September 14, 2024), and CEDS v2025-04 (last access: December 18, 2025).

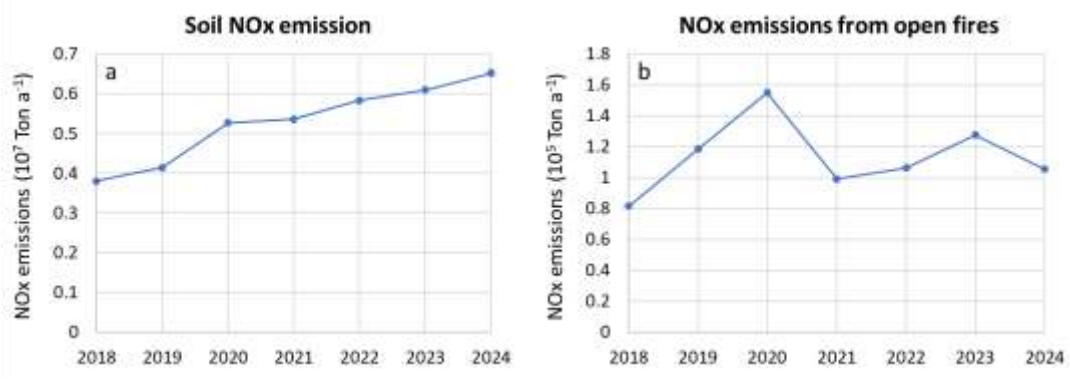


Figure S2. Changes in NO_X emissions from soil and open fires. (a) NO_X emissions from soil in summer from 2018 to 2024 over mainland China. (b) NO_X emissions from open fires in summer from 2018 to 2024 over mainland China.

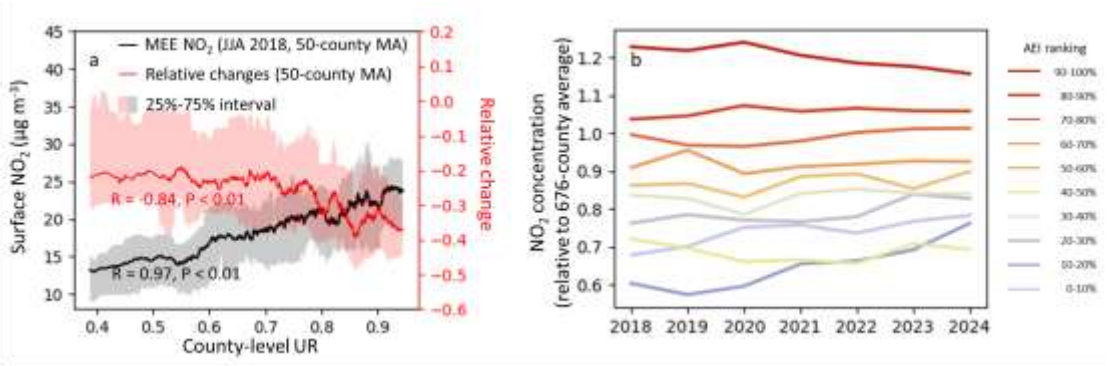


Figure S3. County-level surface NO_2 concentrations based on MEE monitoring, their relative changes alongside urbanization rates, and changes in decile bins ranked by county-level AEI. (a) County-level surface NO_2 concentrations (daily mean) from the MEE monitoring network in summer 2018 (black line) and their relative changes from 2018 to 2024 (red line), as a function of urbanization rates (URs). The data are shown after moving average of 50 counties ranked by URs. (b) Mean surface NO_2 concentrations in different years from MEE over counties in each decile bin ranked by county-level AEI in 2018. The data are normalized by the 676-county average. The NO_2 measurements here do not correct for contamination by other nitrogen species.

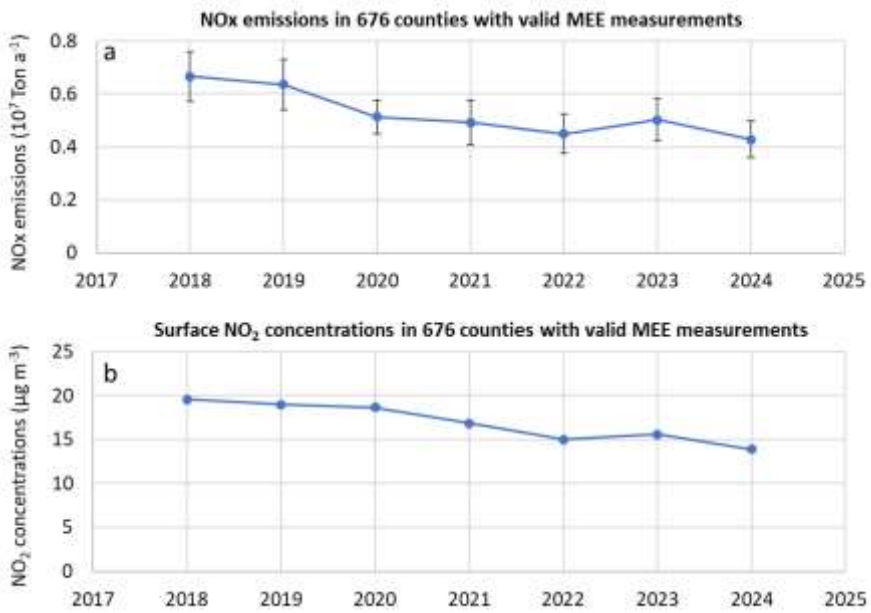


Figure S4. Changes in NO_X emissions and surface NO_2 concentrations in counties with valid MEE monitoring. (a) Summertime NO_X emissions in the 676 counties with valid ground-based monitoring from 2018 to 2024. The error bars denote the 1-σ uncertainties. (b) Summertime daily mean surface NO_2 concentrations averaged over the 676 counties with valid ground-based monitoring from 2018 to 2024. The NO_2 measurements here do not correct for contamination by other nitrogen species.

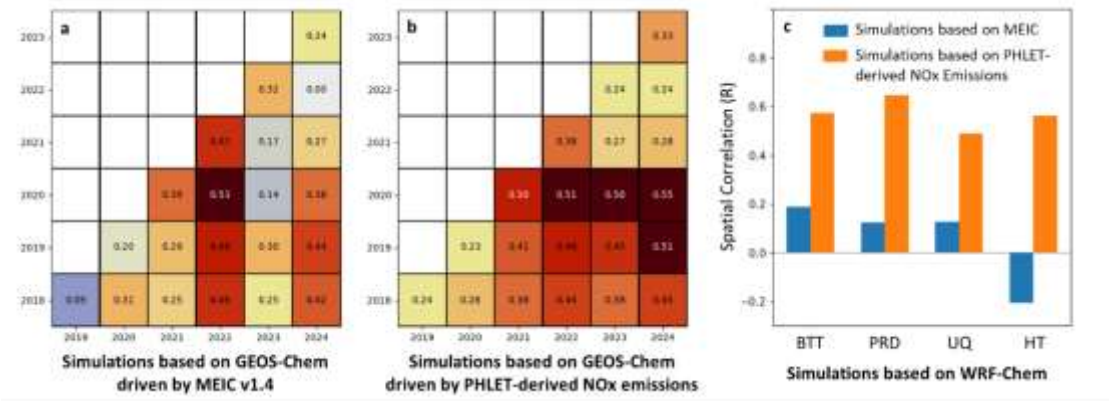


Figure S5. Spatial correlation between changes of near-surface NO_2 in June based on MEE measurements and CTM simulations. (a-b) Interannual changes (from years in y-axis to years in x-axis) derived from MEE measurements and GEOS-Chem simulations driven by NO_X emissions from either MEIC v1.4 (a) or PHLET inversion (b). (c) NO_2 changes (from 2018 to 2024) derived from MEE measurements and WRF-Chem simulations driven by NO_X emissions from either MEIC v1.4 or PHLET inversion. BTT: Beijing-Tianjin-Tangshan region; PRD: the Pearl River Delta; HT: the Hetao region; UQ: the Urumqi area.

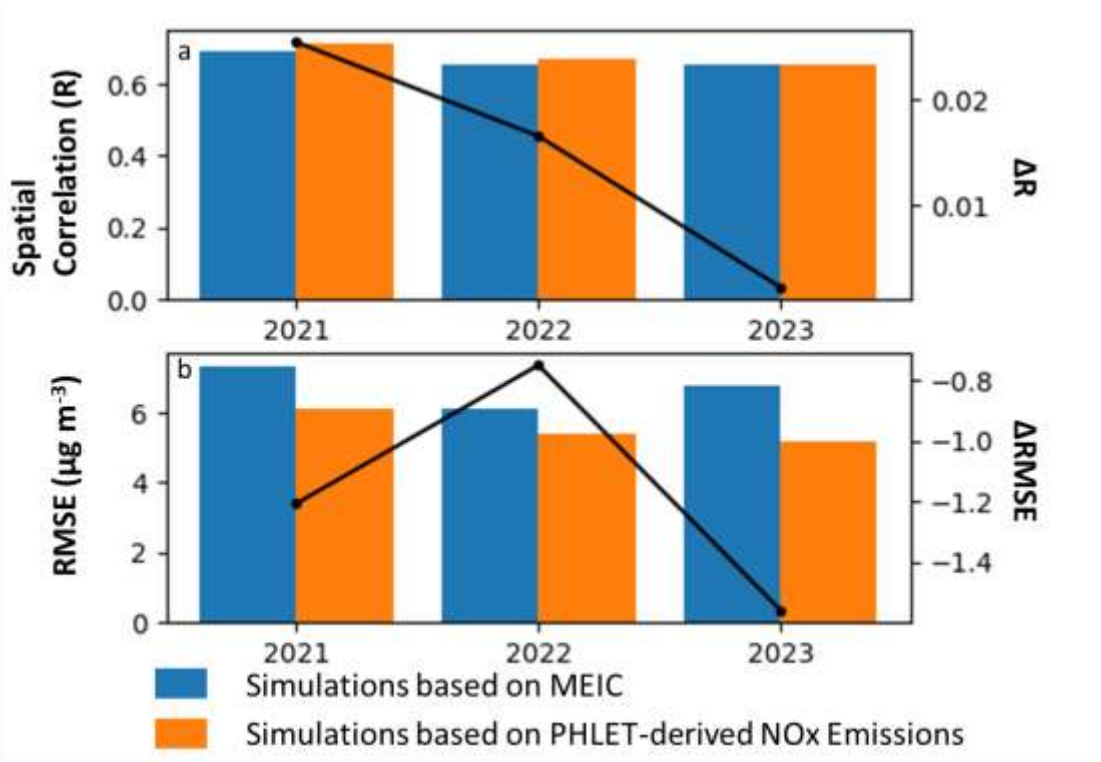


Figure S6. Evaluation of PHLET-derived NO_X emission using GEOS-Chem with MEIC v2.0. Here we show spatial correlations (a) and RMSEs (b) between contamination-corrected MEE measurements and GEOS-Chem simulations, based on MEIC v2.0 and PHLET-derived NO_X emissions, respectively, for monthly daily average NO_2 concentrations in June from 2021 to 2023. The black lines indicate the differences between the PHLET- and MEIC-driven simulations.

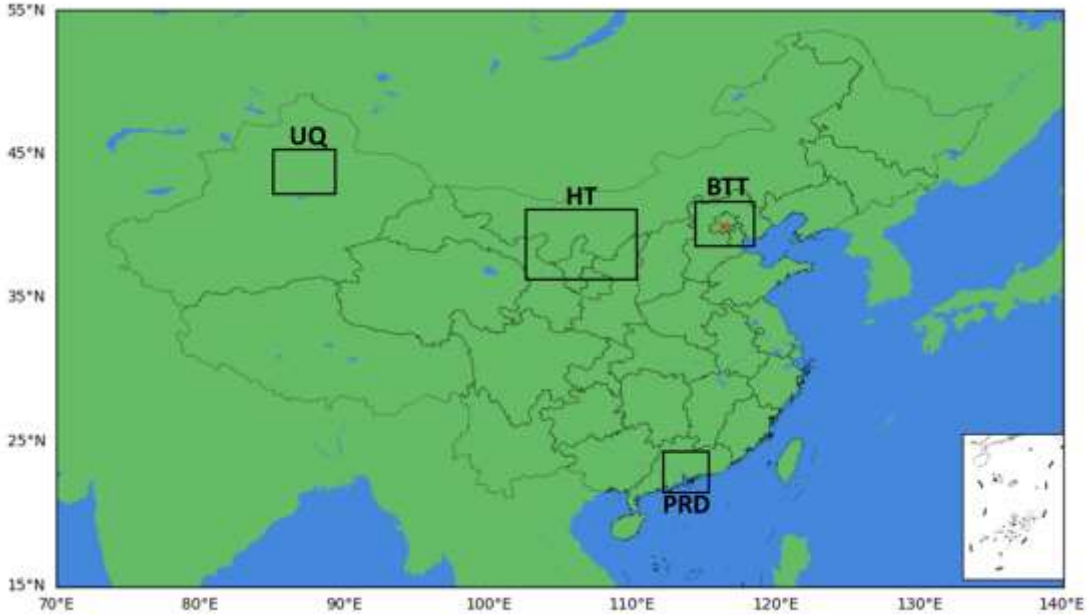
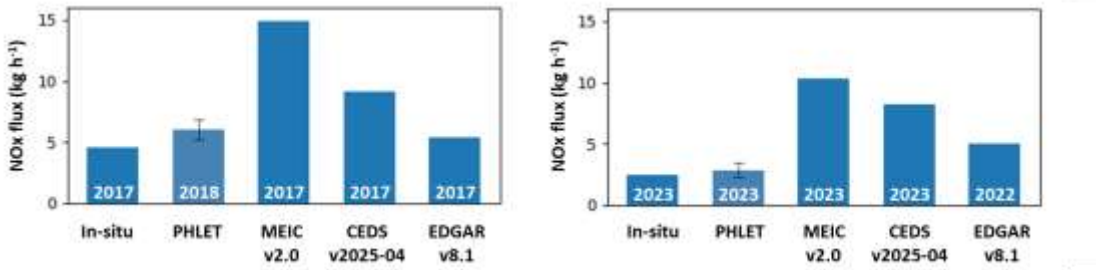


Figure S7. Domains of the 3-km-resolution WRF-Chem simulations. The location of the eddy-covariance flux tower is also marked (red cross). BTT: Beijing-Tianjin-Tangshan region; PRD: the Pearl River Delta; HT: the Hetao region; UQ: the Urumqi area.



62

63 **Figure S8.** Comparison with in-situ flux measurements from an eddy-covariance tower.
64 Emissions for the comparison are derived from PHLET and widely-used inventories
65 including MEIC v2.0, CEDS v2025-04, and EDGAR v8.1. The footprints of the tower
66 flux measurements are applied to each of the emission datasets. Error bars for PHLET
67 represent 1-σ inversion uncertainty. PHLET inversion results from the years closest to
68 the flux measurements are adopted.

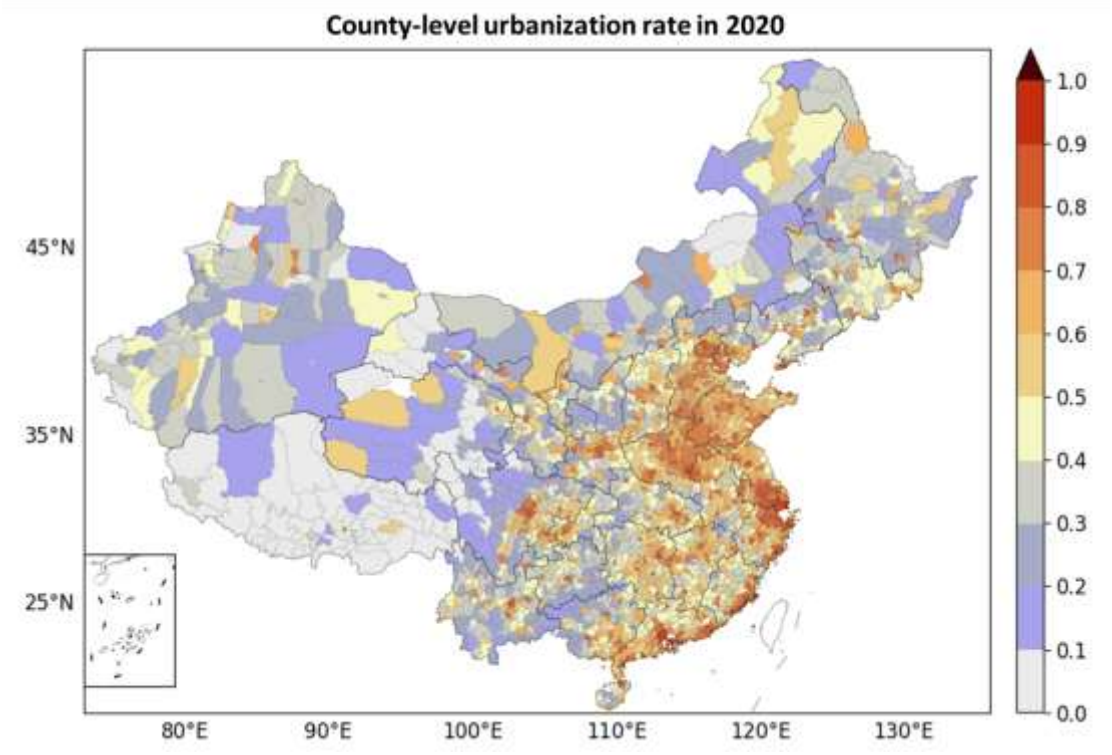


Figure S9. County-level urbanization rates in 2020.

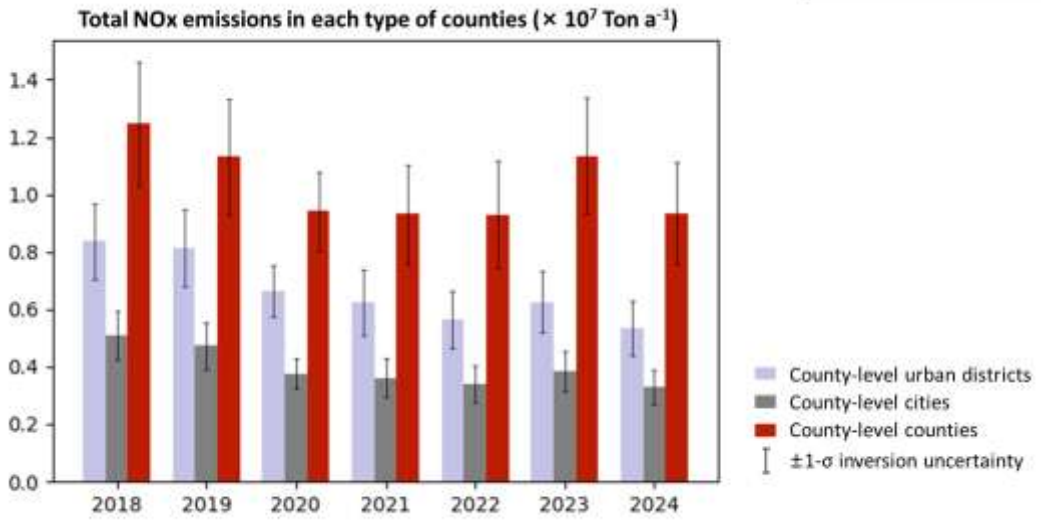
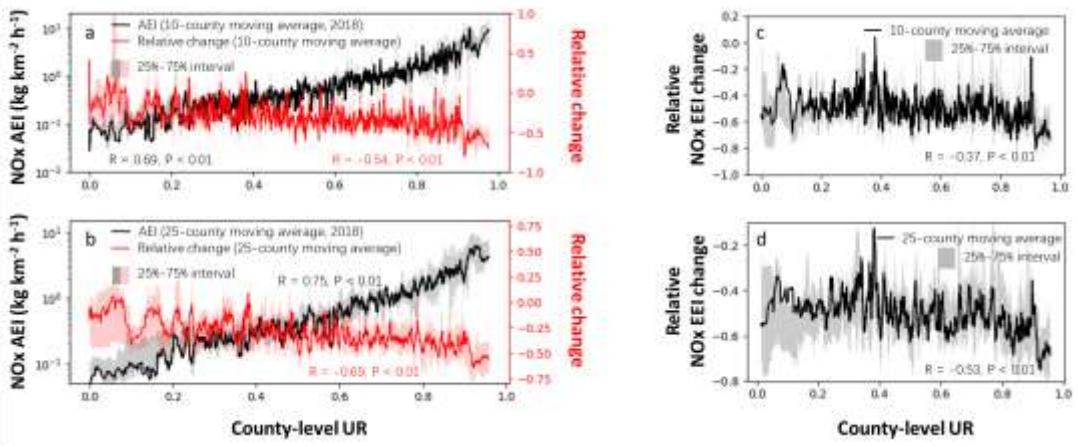
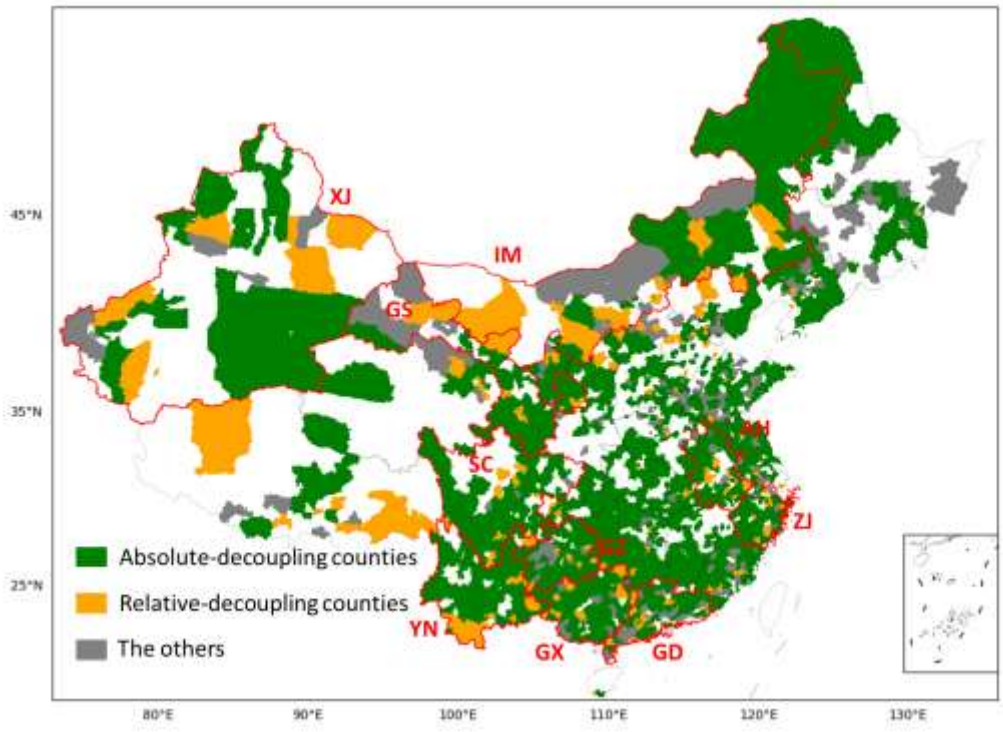


Figure S10. The NO_X emission variations for each county type. The county types include urban districts, county-level cities, and counties, and the data cover 2018–2024. Data are shown with 1-σ uncertainties.



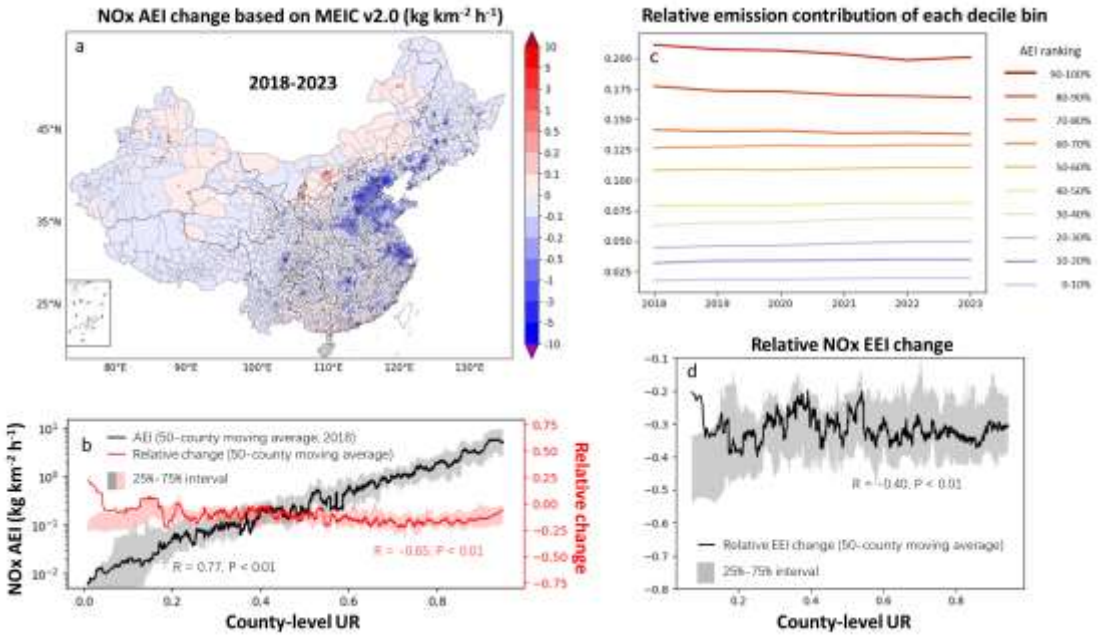
75

76 **Figure S11.** Sensitivity tests for different moving-window sizes. (a) same as Fig. 5c,
77 but using a moving-window size of 10 counties; (b) same as Fig. 5c, but using a moving-
78 window size of 25 counties; (c) same as Fig. 7, but using a moving window size of 10
79 counties; (d) same as Fig. 7, but using a moving window size of 25 counties.



80

81 **Figure S12.** Distribution of counties with different extents of emission-economy
82 decoupling. Blank areas denote counties without available GDP data. The three regions
83 where relative-decoupling counties are mainly located are marked: Xinjiang (XJ),
84 Gansu (GS) and Inner Mongolia (IM) in northwestern China; Sichuan (SC), Yunnan
85 (YN), Guizhou (GZ), Guangxi (GX) and Guangdong (GD, also marked as PRD in Fig.
86 5a) in the south; Anhui (AH) and Zhejiang (ZJ) in eastern China.



87

88 **Figure S13.** County-scale emission characteristics derived from MEIC. MEIC v2.0 is
89 adopted. (a) Changes in county-level NO_X AEIs from 2018 to 2023; (b) County-level
90 NO_X AEIs in 2018 (black line, shown on a logarithmic scale) and relative changes in
91 county-level AEIs from 2018 to 2023 (red line) as a function of urbanization rates (URs);
92 (c) Relative contributions of NO_X emissions from counties in each decile bin ranked by
93 county-level AEI in 2018; (d) Relative NO_X EEI changes, driven by GDP growth and
94 emission reductions, as a function of URs.

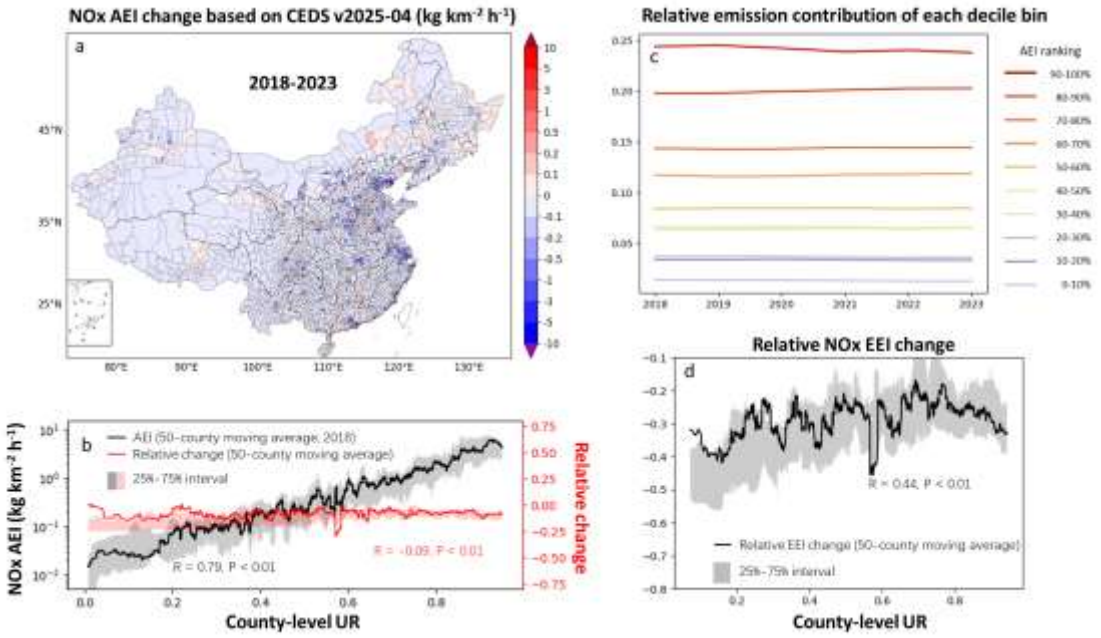
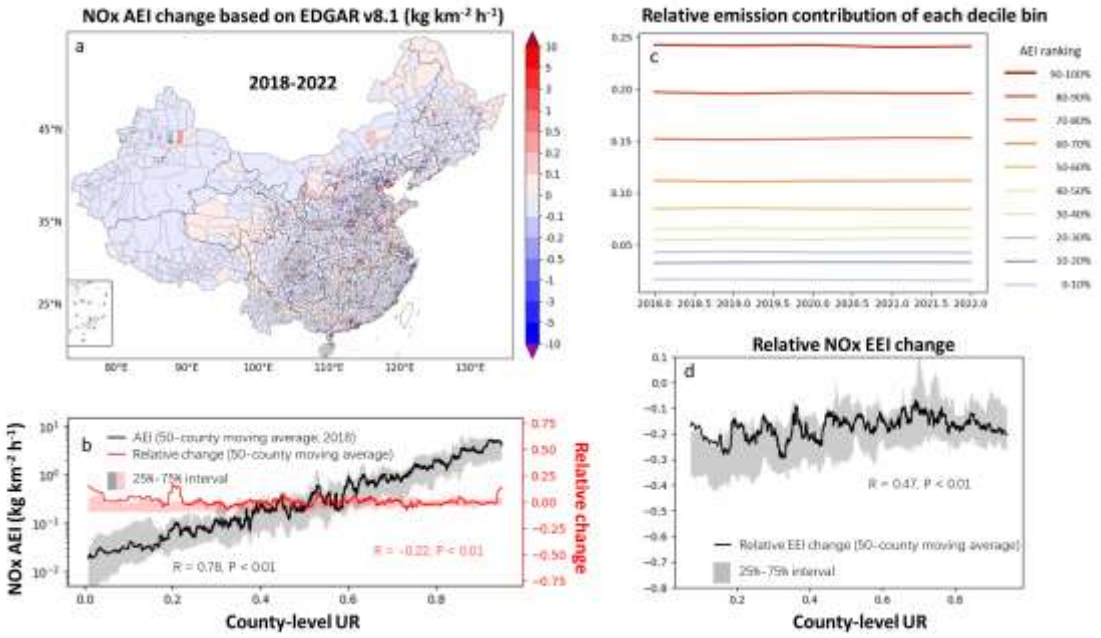


Figure S14. County-scale emission characteristics derived from CEDS. CEDS v2025-04 (available for 2018–2023) is adopted. (a) Changes in county-level NO_X AEIs from 2018 to 2023; (b) County-level NO_X AEIs in 2018 (black line, shown on a logarithmic scale) and relative changes in county-level AEIs from 2018 to 2023 (red line) as a function of urbanization rates (URs); (c) Relative contributions of NO_X emissions from counties in each decile bin ranked by county-level AEI in 2018; (d) Relative NO_X EEI changes, driven by GDP growth and emission reductions, as a function of URs.



103

104 **Figure S15.** County-scale emission characteristics derived from EDGAR. EDGAR
105 v8.1 (available for 2018–2022) is adopted. (a) Changes in county-level NO_X AEIs from
106 2018 to 2022; (b) County-level NO_X AEIs in 2018 (black line, shown on a logarithmic
107 scale) and relative changes in county-level AEIs from 2018 to 2022 (red line) as a
108 function of urbanization rates (URs); (c) Relative contributions of NO_X emissions from
109 counties in each decile bin ranked by county-level AEI in 2018; (d) Relative NO_X EEI
110 changes, driven by GDP growth and emission reductions, as a function of URs.

Tables

Table S1. Statistical evaluation of GEOS-Chem simulations driven by the MEIC v1.4 and PHLET-derived NO_X emissions. The simulations were conducted for June of each year and evaluated against contamination-corrected MEE observations. Statistics include the regression slope, intercept, mean bias (MB), RMSE, and spatial correlation coefficient (R). Because the MEE concentrations are corrected following Eq. 1, the biases depend largely on the empirical coefficients (0.35 and 0.95 in Eq. 1). Therefore, RMSE and R are primarily used in our comparison.

		2018	2019	2020	2021	2022	2023	2024
R	PHLET	0.70	0.71	0.77	0.71	0.67	0.66	0.68
	MEIC	0.70	0.69	0.72	0.70	0.65	0.66	0.66
RMSE (μg m^{-3})	PHLET	6.4	7.0	6.4	6.1	5.4	5.2	4.5
	MEIC	8.6	9.9	8.0	8.1	7.2	8.9	7.4
Mean bias (μg m^{-3})	PHLET	-1.6	-0.7	-4.2	-4.0	-3.0	-2.3	-2.5
	MEIC	-1.1	0.3	-2.0	-1.4	-0.9	1.0	0.3
Slope	PHLET	0.55	0.48	0.68	0.66	0.58	0.58	0.65
	MEIC	0.42	0.36	0.45	0.41	0.37	0.33	0.34
Intercept (μg m^{-3})	PHLET	7.4	7.6	7.3	7.1	6.3	6.2	5.1
	MEIC	8.7	8.8	8.5	8.4	7.2	7.7	6.6

Table S2. Statistical comparison of county-level NO_X emissions between the CAQIEI and PHLET-derived emissions, and between CAQIEI and bottom-up inventories. The comparisons cover counties with MEE monitoring sites.

	R	RMSE (10^3 Ton a^{-1})	Mean Bias (10^3 Ton a^{-1})	Slope	Intercept (10^3 Ton a^{-1})
PHLET	0.57	9.7	4.7	0.67	-2.3
MEIC v1.4	0.14	13.7	6.4	0.15	1.1
CEDS v2025-04	0.24	13.4	6.4	0.25	0.3
EDGAR v8.1	0.16	14.4	6.2	0.15	1.2

Table S3. Comparison of urbanization and emission characteristics between counties with and without available GDP data.

	1,779 counties with GDP data	**1,063 counties without GDP data**
Urbanization rate	0.65	0.66
NO_X AEI in 2018 ($kg\ km^{-2}\ h^{-1}$)	0.33 ± 0.06	0.29 ± 0.05
Total summertime NO_X emission in 2024 ($10^7\ Ton\ a^{-1}$)	1.13 ± 0.19	0.67 ± 0.11
Fraction of emission-increasing counties	16.5%	14.9%